GABAergic circuits mediate the reinforcement-related signals of striatal cholinergic interneurons

Daniel F English[1], Osvaldo Ibanez-Sandoval[1], Eran Stark[1], Fatuel Tecuapetla[1,3], György Buzsáki[1], Karl Deisseroth[2], James M Tepper[1] & Tibor Koos[1]

Neostriatal cholinergic interneurons are believed to be important for reinforcement-mediated learning and response selection by signaling the occurrence and motivational value of behaviorally relevant stimuli through precisely timed multiphasic population responses. An important problem is to understand how these signals regulate the functioning of the neostriatum. Here we describe the synaptic organization of a previously unknown circuit that involves direct nicotinic excitation of several classes of GABAergic interneurons, including neuroptide Y–expressing neurogilaform neurons, and enables cholinergic interneurons to exert rapid inhibitory control of the activity of projection neurons. We also found that, *in vivo*, the dominant effect of an optogenetically reproduced pause-excitation population response of cholinergic interneurons was powerful and rapid inhibition of the firing of projection neurons that is coincident with synchronous cholinergic activation. These results reveal a previously unknown circuit mechanism that transmits reinforcement-related information of ChAT interneurons in the mouse neostriatal network.

The neostriatum is critical for the reinforcement-mediated acquisition and selection of adaptive behavioral responses[1,2]. These functions require neuronal representation of information about the occurrence and motivational value of external stimuli that are provided by two major neuromodulatory systems: midbrain dopaminergic neurons and local cholinergic, or choline acetyltransferase (ChAT)-expressing, interneurons. These two neuron populations exhibit coincident firing rate changes in response to the presentation of unpredicted or the omission of predicted primary reinforcement, as well as to cues that predict these stimuli, and together encode the value, magnitude and expectation probability of these events[2–8]. More specifically, ChAT interneurons exhibit multiphasic population responses, which consist of a brief (200–300 ms) cessation of firing, termed the pause response, and, depending on the nature of the stimulus and its behavioral context, an immediately following and sometimes a preceding period of brief semi-synchronous excitation[3,4,6–9]. An important question is how these population responses regulate the functioning of the neostriatal network. Given the multiphasic nature of these responses and the absence of spatial segregation of ChAT interneurons, classical methods have not been adequate to address this issue. We used optogenetic excitatory and inhibitory tools to reproduce synchronous excitation and pause-excitation firing patterns of ChAT interneurons, and found that ChAT interneurons activate parallel GABAergic circuits that mediate powerful inhibition of striatal projection neurons *in vitro* and *in vivo*.

RESULTS

ChAT interneurons activate GABAergic inhibition in SPNs

The effects of synchronous activation of ChAT interneurons were examined using a channelrhodopsin-2–yellow fluorescent protein (ChR2-YFP) fusion construct expressed in ChAT interneurons with viral-mediated transfer of a Cre-*loxP* controlled transgene. We verified ChR2 expression specificity with immunocytochemistry and found ChAT expression in ~98.7% (81 of 82) of ChR2-YFP+ neurons (**Fig. 1a**). Postsynaptic responses to activation of cholinergic interneurons (**Fig. 1b**) were investigated *in vitro* in brains slices prepared from adult (postnatal day 60–390) mice using standard methods[10]. In all spiny projection neurons (SPNs) examined ($n = 94$), synchronous activation of ChAT interneurons elicited a polysynaptic $GABA_A$ receptor–mediated inhibitory postsynaptic potential or current (IPSP or IPSC; **Fig. 1c,d**) involving nicotinic receptors, as the response was blocked by selective antagonists of $GABA_A$ and type-2 nicotinic receptors (10 µM, bicuculline and between 100 nM and 10 µM dihydro-β-erythroidine (DHβE), respectively, $n = 10$; **Fig. 1d**), but not by antagonists of AMPA-type glutamatergic receptors (10 µM 6-cyano-7-nitroquinoxaline-2,3-dione (CNQX), $n = 10$; **Supplementary Fig. 1**) or muscarinic receptors (10 µM atropine, $n = 3$, data not shown). The IPSC was characterized by a relatively long onset latency and short rise time (11 ± 1.7 and 5.0 ± 0.6 ms, respectively, $n = 11$), and exhibited a peak conductance of 2.8 ± 0.9 nS. In current clamp, optical stimulation elicited large-amplitude IPSPs in SPNs ($n = 20$) that efficiently blocked action potential generation and decreased the momentary firing rate of projection neurons in a rate-dependent manner (**Fig. 1c** and **Supplementary Fig. 2**).

We also investigated the contribution of single ChAT interneurons to the inhibition of SPNs using paired recordings. In ~50% of pairs ($n = 21$), single spikes in ChAT interneurons elicited bicuculline- (10 µM, $n = 4$) and DHβE-sensitive (10 µM, $n = 3$) small IPSCs in SPNs (<20 pA, CsCl internal solution, E[Cl⁻] = −10 mV; **Supplementary Fig. 3**).

[1]Center for Molecular and Behavioral Neuroscience, Rutgers University, Newark, New Jersey, USA. [2]Department of Bioengineering, Stanford University, Stanford, California, USA. [3]Present address: Neurobiology of Action, Instituto Gulbenkian de Ciencia, Oeiras, Portugal. Correspondence should be addressed to T.K. (tibkoos@yahoo.com).

Figure 1 Characterization of GABAergic IPSCs elicited in SPNs with optogenetic stimulation of ChAT interneurons. (**a**) Confocal images of a ChR2-YFP–expressing neuron (top left) immunostained for ChAT (middle; bottom, overlay). A larger field is shown at the right. (**b**) Top, optically elicited action potential in a ChAT interneuron. Bottom, a cell-attached recording of spontaneous activity and optically evoked action potentials (red arrows) of a ChAT interneuron. (**c**) Optogenetically elicited IPSPs in an SPN (arrow) efficiently blocked firing induced by current injection. Bottom trace, corresponding IPSC (V_{hold} = –80 mV). (**d**) Optogenetically elicited IPSCs in two SPNs (blue traces) were blocked by bicuculline (Bic, left) or DHβE (right, red traces). (**e**) Kinetic components of the compound IPSC. Left, three distinct components of the IPSC exhibiting different τ_{decay} values. Right, non-monotonic transition between the fIPSC and the sIPSC. Note the negative inflection following the transition (red arrowhead). Inset, decomposition of the compound IPSC (black trace) into a fIPSC (blue trace) and sIPSC (red trace). (**f**) Independent trial-to-trial amplitude variance of the fIPSC and the sIPSC. Left, overlay of four responses exhibiting identical sIPSC, but different fIPSC, components (colored arrows point to fIPSC peaks). Shaded areas are averaging windows. Middle, variable sIPSC components. Right, relative sIPSC amplitudes plotted against corresponding relative peak fIPSC amplitudes (n = 5). Red line is linear regression (n.s., not significant, P > 0.2). (**g**) Inhibition of GAT-1 selectively prolonged the sIPSC. Note that the fIPSC was unaffected (arrow and inset). Red arrow, transition point of the response components. In all figures, the blue bars represent optical stimuli.
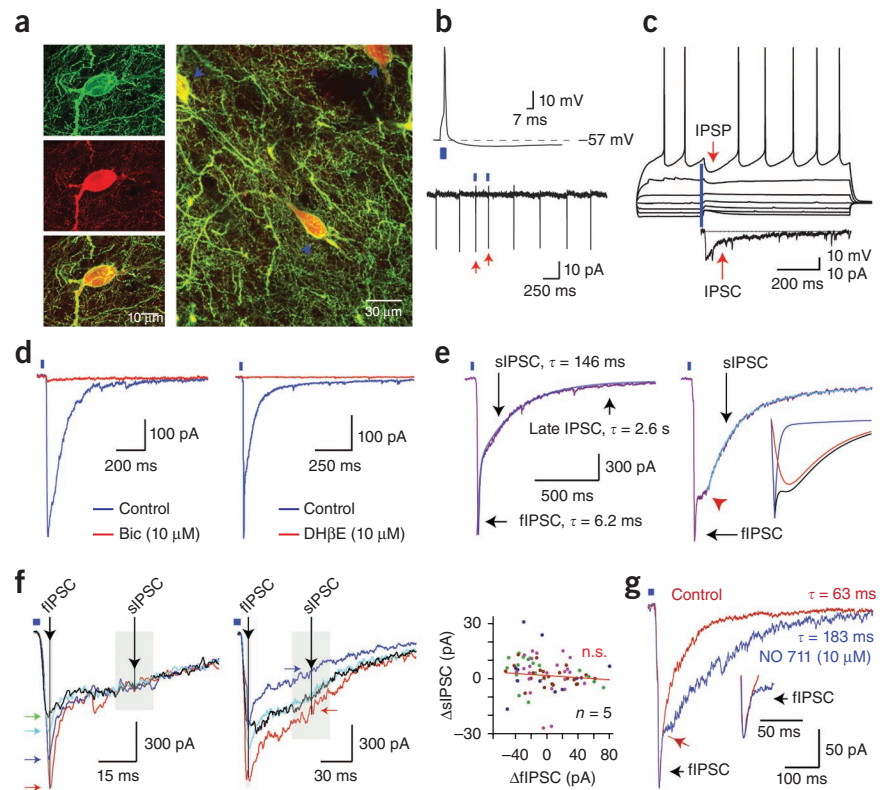
GABAergic inhibition in SPNs involves multiple mechanisms

The optically elicited IPSCs in SPNs were multiphasic, consisting of three kinetically distinct phases characterized by τ_{decay} values of 5.2 ± 1.8, 96 ± 11.7 and 906 ± 106 ms (n = 6). We refer to the first two components as fast and slow IPSCs (fIPSC and sIPSC; **Fig. 1e**). Because of its small amplitude (~20 pA), we chose not to further investigate the mechanism underlying the slowest component. In about one-third of the SPNs, the transition between these response components was not monotonic, but the sIPSC was introduced by a clear inflection (**Fig. 1e**), suggesting that the compound response represents the superposition of two distinct GABAergic responses, a typical fast IPSC and a slowly rising and slowly decaying GABAergic response, which was less apparent when the onset of the sIPSC was obscured by larger or slower fIPSC components (**Fig. 1e**). To more directly test the involvement of two distinct mechanisms, we examined the trial-to-trial correlation of the amplitudes of the fIPSC and sIPSC components (**Fig. 1f**). Close examination of individual responses and linear regression analysis revealed that the amplitude of the fIPSC and the sIPSC varied independently (**Fig. 1f**). This excludes the possibility that the sIPSC represents a distinct kinetic phase of activation of the same receptors that mediate the fIPSC or that the two responses are secondary to the release of GABA from the same axon terminals reaching functionally distinct receptor populations.

We also noted that the sIPSC appeared to be similar to a form of slow GABA$_A$ receptor–mediated inhibition (GABA$_A$ slow) first described in the hippocampus and the neocortex[11–13]. To test the possibility that the sIPSC is involved in a similar mechanism, we took advantage of the characteristic sensitive dependence of the τ_{decay} of this response on inhibition of GABA transport[14–16], a characteristic

that is not exhibited by conventional GABAergic synapses[16,17]. Application of NO711 (10 μM), a selective inhibitor of GAT-1, markedly increased the τ_{decay} of the sIPSC from 57.5 ± 2.5 ms to 185.2 ± 17.5 ms (322%, n = 4, Wilcoxon test, P = 0.02; **Fig. 1g**). In contrast, the time course of the fIPSC was not affected (control, 10.5 ± 1.7 ms; NO711, 9.3 ± 4.9 ms; n = 3, P = 0.6, Wilcoxon test; **Fig. 1g**). Together, these results indicate that the fIPSC and the sIPSC originate from separate and biophysically distinct mechanism, including a component that resembles GABA$_A$ slow.

NPY-NGF interneurons mediate the sIPSC in SPNs

We recently demonstrated the existence of a class of neuropeptide Y (NPY)-expressing interneurons in the neostriatum, the NPY neurogliaform (NPY-NGF interneurons), that are morphologically and electrophysiologically distinct from known NPY-expressing plateau depolarization–low threshold spike (NPY-PLTS) neurons[18]. Notably, unlike NPY-PLTS neurons, which very rarely contact SPNs[19], NPY-NGF interneurons elicit an IPSC in most nearby SPNs (~84%) and this response is kinetically very similar to GABA$_A$ slow[18] (the comparative properties of NPY-NGF and NPY-PLTS interneurons are illustrated in **Supplementary Figs. 4** and **5**). In addition to eliciting a slow GABAergic IPSC, NPY-NGF interneurons exhibit marked electrophysiological and morphological similarities to NPY-expressing neurogliaform neurons in the neocortex[15] and hippocampus[14], which (together with Ivy cells) are the primary source of GABA$_A$ slow in these brain areas[20].

We hypothesized that NPY-NGF interneurons may be responsible for the sIPSC component in SPNs. To examine this possibility, we first obtained triple and paired recordings to determine whether NPY-NGF
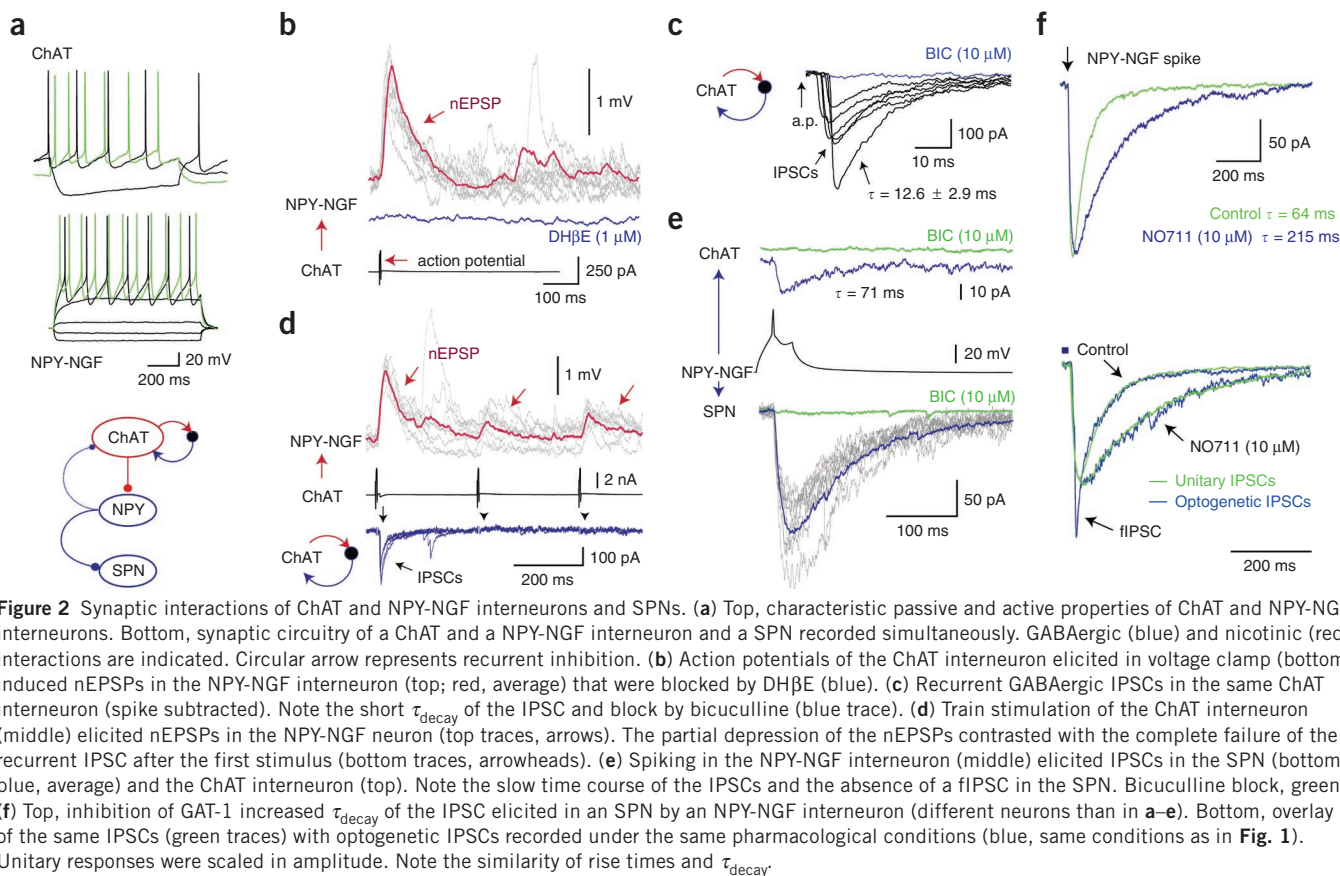
Figure 2 Synaptic interactions of ChAT and NPY-NGF interneurons and SPNs. (**a**) Top, characteristic passive and active properties of ChAT and NPY-NGF interneurons. Bottom, synaptic circuitry of a ChAT and a NPY-NGF interneuron and a SPN recorded simultaneously. GABAergic (blue) and nicotinic (red) interactions are indicated. Circular arrow represents recurrent inhibition. (**b**) Action potentials of the ChAT interneuron elicited in voltage clamp (bottom) induced nEPSPs in the NPY-NGF interneuron (top; red, average) that were blocked by DHβE (blue). (**c**) Recurrent GABAergic IPSCs in the same ChAT interneuron (spike subtracted). Note the short τ_{decay} of the IPSC and block by bicuculline (blue trace). (**d**) Train stimulation of the ChAT interneuron (middle) elicited nEPSPs in the NPY-NGF neuron (top traces, arrows). The partial depression of the nEPSPs contrasted with the complete failure of the recurrent IPSC after the first stimulus (bottom traces, arrowheads). (**e**) Spiking in the NPY-NGF interneuron (middle) elicited IPSCs in the SPN (bottom; blue, average) and the ChAT interneuron (top). Note the slow time course of the IPSCs and the absence of a fIPSC in the SPN. Bicuculline block, green. (**f**) Top, inhibition of GAT-1 increased τ_{decay} of the IPSC elicited in an SPN by an NPY-NGF interneuron (different neurons than in **a**–**e**). Bottom, overlay of the same IPSCs (green traces) with optogenetic IPSCs recorded under the same pharmacological conditions (blue, same conditions as in **Fig. 1**). Unitary responses were scaled in amplitude. Note the similarity of rise times and τ_{decay}.

interneurons received nicotinic synaptic excitation from ChAT interneurons and whether the same NPY-NGF interneurons elicited IPSCs similar to the sIPSC component in SPNs using NPY–enhanced GFP (EGFP) transgenic reporter mice (**Fig. 2a**). In 8 of 14 instances of simultaneously recorded ChAT and NPY-NGF interneurons ($n = 8$ ChAT, NPY-NGF and SPN triples; $n = 6$ pairs), a postsynaptic response could be elicited in the NPY-NGF neurons by single action potentials in the ChAT interneuron (57% connectivity; **Fig. 2b**). Although the ChAT interneurons were activated in voltage clamp in most cases, action potentials triggered in current clamp elicited similar postsynaptic responses (**Supplementary Fig. 6**). The response had an average amplitude of 0.96 ± 0.7 mV (range, 0.28–2.27 mV), rise time of 14.7 ± 5.3 ms (range, 9.0–24.7 ms), decay time constant of 75.6 ± 40.2 ms (range, 27.8–147 ms), onset latency of 3.6 ± 1.6 ms and exhibited no transmission failures (**Fig. 2b**). The response was a type-2 receptor–mediated nicotinic excitatory postsynaptic potential (nEPSP), as it was blocked by DHβE (200 nM, $n = 3$; 1 μM, $n = 2$; **Fig. 2b**), but not by glutamatergic AMPA or GABA$_A$ receptor antagonists (10 μM CNQX, $n = 3$; 10 μM bicuculline, $n = 4$; data not shown). Stimulation of ChAT interneurons also triggered recurrent IPSCs (**Fig. 2c**). Train stimulation ($n = 2$, 3.33 Hz, 3 spikes) revealed substantial, but incomplete, depression of the nEPSP (60–75%, $n = 2$; **Fig. 2d**) that contrasted with the complete use-dependent suppression of recurrent GABAergic inhibition in simultaneously recorded ChAT interneurons (**Fig. 2d**). Among the eight NPY-NGF interneurons shown to receive nicotinic innervation from a ChAT interneuron, four out of five tested interneurons elicited IPSCs in SPNs (**Fig. 2e**). The IPSC elicited by NPY-NGF interneurons in SPNs ($n = 11$, 4 from triple recordings and 7 from additional pairs) was similar to GABA$_A$ slow and exhibited an average amplitude of 155.7 ± 160.7 pA (range,

17.6–534 pA), rise time of 9.5 ± 4.9 ms (range, 3.6–17.8 ms) and τ_{decay} of 65.8 ± 14.98 ms (range, 37–93 ms; CsCl internal solution; **Fig. 2e,f** and **Supplementary Fig. 5**). The probability of connectivity to SPNs was very high 11 of 14 (78%). The τ_{decay} of the IPSC (68.7 ± 12.1 ms; range, 56–93 ms) did not differ significantly from the τ_{decay} of the sIPSC in SPNs elicited with optogenetic stimulation of ChAT interneurons (96 ± 28.7 ms, Wilcoxon test, $P > 0.05$, $n = 6$). Notably, the IPSCs elicited by NPY-NGF interneurons never included fast IPSC components or exhibited biphasic decay (**Fig. 2e,f** and **Supplementary Fig. 5**).

To further test the contribution of NPY-NGF interneurons to the sIPSC, we next tested the effect of GAT-1 inhibition. NO711 increased the τ_{decay} of the IPSC in a dose-dependent manner from 61.3 ± 9.2 ms to 205.6 ± 28 ms at 10 μM (336%, $n = 3$; **Fig. 2f**) and from 92 ± 28.3 ms to 1310 ± 975 ms at 50 μM ($n = 2$, $P = 0.02$, Wilcoxon test; data not shown). The effects of NO711 on the optogenetic sIPSC and the IPSC elicited by NPY-NGF neurons were essentially identical at the same drug concentration (322% versus 336%; **Fig. 2f**).

In addition, we observed that in 3 of 14 pairs (21%), NPY-NGF interneurons elicited a GABAergic IPSC in ChAT interneurons (**Fig. 2e**). This response was blocked by bicuculline ($n = 2$; **Fig. 2e**) and exhibited small amplitudes (9.4 ± 8 pA; range, 2.8–18.5 pA; E[Cl$^-$] ≈ −10 mV). Notably, NPY-NGF neurons could not mediate recurrent inhibition of ChAT interneurons because this IPSC and the recurrent IPSCs exhibited very different τ_{decay} values (77 ± 37 ms ($n = 3$) and 19.2 ± 12.7 ms ($n = 8$), respectively; $P = 0.014$, Wilcoxon test; **Fig. 2c,e**) and because activation of single ChAT interneurons never elicited action potentials or nEPSPs approaching spike threshold in NPY-NGF neurons, although recurrent inhibition was frequently triggered (**Fig. 2c** and **Supplementary Fig. 7**). Finally, electrotonic coupling
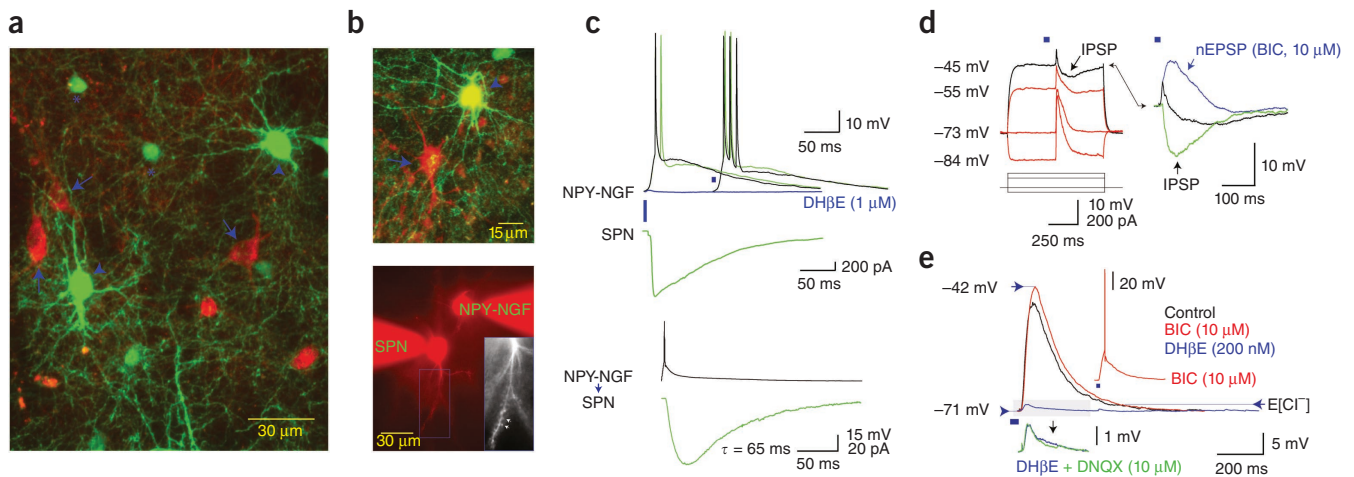
Figure 3 Optogenetic activation of ChAT interneurons elicits nEPSPs and GABAergic IPSPs and triggers action potential firing in NPY-NGF interneurons. (**a**) Confocal image of ChAT interneurons expressing ChR2-mCherry (arrows) and two EGFP-expressing NPY-NGF neurons (arrowheads) in a *Chat-cre; Npy-GFP* mouse. (**b**) Top, confocal images of a NPY-NGF interneuron (arrowhead) and a simultaneously recorded nearby SPN intracellularly labeled with Alexa 594 (arrow). Bottom, photomicrographs of the neurons during recording. Inset, high magnification showing SPN dendritic spines (arrows, same neurons as shown in **c**). (**c**) Top, optical stimulation of ChAT interneurons elicited large amplitude depolarizations and action potentials in a NPY-NGF interneuron that were blocked by DHβE (blue trace). Simultaneously elicited optogenetic compound IPSC in the SPN (bottom green trace). Bottom, single action potential in the NPY-NGF neuron (black trace) elicited a slow IPSC in the SPN (green trace). (**d**) EPSP-IPSC sequence elicited with optical stimulation of ChAT interneurons in an NPY-NGF neuron (different neuron than those shown in **b**, **c** and **e**). Left, reversal of the IPSP (arrow). Right, the IPSP (green trace), the compound response (black trace) and the isolated nEPSP (blue trace) were recorded at ~−45 mV. Note the large amplitude and slow time course of the isolated IPSP. (**e**) The compound optogenetic response of another NPY-NGF interneuron (black trace) was gradually increased in amplitude by application of bicuculline (red trace), leading to action potential firing (top inset). The isolated nEPSP (red trace) was blocked by ~95% by 200 nM DHβE (blue trace). The residual response (blue trace, bottom inset) was not sensitive to 6,7-dinitroquinoxaline-2,3-dione (DNQX, green trace).

was also observed in one of two pairs of NPY-NGF interneurons (**Supplementary Fig. 5**). These observations suggest the existence of a highly interconnected circuitry between ChAT and NPY-NGF interneurons and SPNs in which NPY-NGF neurons receive dense cholinergic excitatory input from ChAT interneurons and provide widespread innervation of SPNs using slow GABAergic inhibition.

We next tested whether synchronous activation of ChAT interneurons elicited action potentials in NPY-NGF interneurons using slices from double transgenic *Chat-cre; Npy-EGFP* mice, which allow selective optogenetic stimulation of ChAT interneurons using targeted ChR2 expression, and visualized recording from NPY-NGF neurons (**Fig. 3a,b**). Optogenetic stimulation of the ChAT interneuron population elicited large-amplitude depolarizing postsynaptic potentials in all of the NPY-NGF neurons that we tested and, in two of seven neurons, triggered one to three action potentials with interspike intervals <10 ms. (**Fig. 3c–e**). Simultaneous recordings from nearby SPNs (*n* = 3) revealed that the postsynaptic responses in the NPY-NGF neurons were accompanied by compound optogenetic IPSCs in the SPNs and that the same NPY-NGF neurons themselves elicited slow GABA$_A$ receptor–mediated responses in the projection neurons (**Fig. 3c**). Reversal potential measurements revealed that the optogenetically elicited postsynaptic response in NPY-NGF interneurons consisted of an early excitatory and a delayed inhibitory component (**Fig. 3d**). The IPSC component, which itself was secondary to nicotinic receptor activation (data not shown), exhibited 4–12-mV amplitudes ($V_m \approx$ −45 mV, E[Cl$^-$] ≈ −69 mV) and was GABA$_A$ receptor mediated (10 μM bicuculline, *n* = 5; **Fig. 3d**). This inhibitory response may be important for limiting the nicotinic activation of NPY-NGF neurons; in one cell that did not fire action potentials in control medium, firing was elicited after GABA$_A$ receptor block (**Fig. 3e**). The pharmacologically isolated excitatory response (*n* = 5) was a nEPSP because it was reduced in amplitude by >95% by DHβE both at 200 nM (*n* = 2) and at 1 μM (*n* = 3; **Fig. 3c,e**). The nEPSP exhibited amplitudes of

8.8–34.2 mV (average, 16.8 ± 10.3 mV), rise time of 16.8 ± 2.2 ms (range, 16.5–21.5 ms) and τ_{decay} of 60.0 ± 8.9 ms (range, 51–71 ms; **Fig. 3e**). No contribution from glutamatergic AMPA receptors was detected (**Fig. 3e**).

FSIs and NPY-PLTS neurons are not activated by ChAT neurons
Other neostriatal interneuron types were tested to see if they could mediate the fIPSC and/or contribute to the sIPSC component of the compound optogenetic IPSC in SPNs. SPNs themselves could be excluded because they lack nicotinic receptors[21] and were not activated in optogenetic experiments (**Fig. 1c**). Fast-spiking interneurons (FSIs) are another major source of inhibition of SPNs[22] (**Fig. 4a**) and represent an important candidate because they express nicotinic receptors[23] and receive cholinergic innervation[24]. Cholinergic stimulation failed to elicit any substantial depolarization (>3 mV) or action potential firing in the recorded FSIs (*n* = 8), despite the presence of IPSCs, including large fIPSC components in nearby SPNs, indicating that FSIs are not involved in the feedforward inhibition of SPNs (**Fig. 4b**). The absence of excitation was not a slice preparation artifact because nicotinic excitatory postsynaptic currents were readily elicited in all NPY-NGF neurons (**Figs. 2 and 3**).

A possible contribution by the sparse input to SPNs from NPY-PLTS interneurons[19] was excluded using the same double transgenic optogenetic strategy that we employed to investigate the role of NPY-NGF interneurons (**Supplementary Fig. 8**). However, these results did not rule out the existence of small depolarizing effects on FSIs and NPY-PLTS interneurons or the possibility that presynaptic facilitation of GABA release from these interneurons contributes to the inhibition of SPNs. Finally, biophysical differences and stimulus intensity–dependent dissociation of the feedforward inhibition of SPNs and recurrent inhibition in ChAT interneurons[25] strongly suggest that these responses were not mediated by the same interneurons (**Supplementary Fig. 7**).

Figure 4 FSIs do not mediate the inhibition of SPNs by ChAT interneurons. (**a**) Paired recording from a synaptically connected FSI and SPN. Intracellularly injected current pulses in the interneuron elicited voltage responses that identified it as an FSI (bottom). Note the typical large-amplitude IPSCs elicited in the SPN (arrows). (**b**) Optical stimulus (blue bar) elicited a compound IPSC, including a large fIPSC in the SPN (blue trace, top), but failed to trigger action potentials or large depolarizing potentials in the FSI (red trace, bottom), as compared with the responses elicited in NPY-NGF neurons in **Figure 3d,g**.
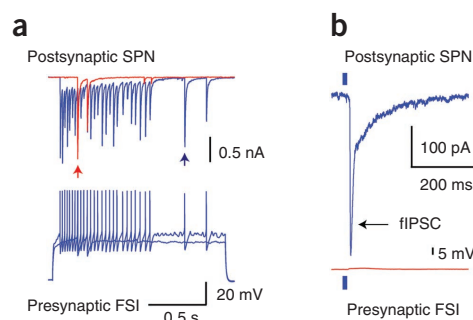
Cholinergic pause-excitation response regulates the firing of SPNs

In behaving primates, the most common reinforcement-related population activity of putative ChAT interneurons is a pause-excitation sequence[3,4,7–9]. The quantitative properties of the postsynaptic effects of the excitatory phase of this population response may not be evaluated adequately using ChR2-mediated synchronous activation alone because this approach does not reproduce the pause-associated reduction in cholinergic tone that may have substantial effects via receptor deactivation[23,26] or recovery from desensitization[27] and because of the possibility of eliciting nonphysiologically enhanced neurotransmitter release and abnormally high extracellular acetylcholine transients resulting from prolonged presynaptic depolarization and Ca^{2+} influx. To overcome these problems, we used optogenetic inhibition to elicit a pause excitation response by taking advantage of the fact that ChAT interneurons respond to brief hyperpolarization with semi-synchronous rebound firing[28]. ChAT interneurons expressing an enhanced variant of *Natronomonas pharaonis* halorhodopsin[29] (eNpHR3.0) exhibited normal intrinsic properties *in vitro* and responded to optical stimuli (green light, 200–300 ms) with hyperpolarizing responses and rebound action potentials (**Fig. 5a,b**). Cell-attached and extracellular recordings revealed that the majority of ChAT interneurons were spontaneously active and generated variable latency rebound firing following optical inhibition (**Fig. 5b–e**) successfully approximating the pause and the typical properties of excitatory population responses of putative ChAT interneurons

recorded *in vivo*[3,4,8,30] (**Fig. 5c**). The optically induced population activity of cholinergic interneurons elicited large-amplitude GABAergic IPSPs in SPNs (**Fig. 5c–e**) that were secondary to the activation of type-2 nicotinic receptors, as shown by DHβE block (200 nM, $n = 5$; **Fig. 5e**). The onset of the response followed the end of the light pulse with a short latency (~50 ms) and was apparently initiated by the first cholinergic rebound spikes (**Fig. 5c,d**). The IPSP effectively blocked action potential generation in SPNs (**Fig. 5c–e**). A minority of the SPNs ($n = 5$) exhibited an additional, more delayed period of inhibition that was similarly blocked by DHβE (200 nM, $n = 2$) and coincided with longer latency rebound activity of some ChAT interneurons (**Fig. 5a,e**). Current recordings revealed that the elicited synaptic response in SPNs resembled the compound response described above (**Fig. 5d**). These latter experiments were conducted using eNpHR1.0-mCherry (see Online Methods), which is not expressed in axons and therefore circumvents any potential effects of direct axon terminal hyperpolarization[29,31].

Finally, we sought to confirm that the pause-excitation activity pattern of ChAT interneurons also exerts inhibitory control on projection neurons *in vivo*. We obtained single and multi-unit recordings in the dorsal striatum of freely moving mice expressing eNpHR3.0 in ChAT interneurons with chronically implanted optrodes containing four movable tetrodes and a fixed, laser-coupled optic fiber. The optical

Figure 5 Optogenetically reproduced pause-excitation population response of ChAT interneurons elicits powerful inhibition in SPNs *in vitro*. (**a**) Photomicrograph of eNpHR3.0-YFP–expressing ChAT interneurons (arrow, arrowhead) labeled intracellularly with Alexa 594 (red). (**b**) Top, responses of an eNpHR3.0-YFP–expressing ChAT interneuron to intracellular current (**a**, arrow). Whole-cell (middle) and cell-attached (bottom) recordings demonstrated spontaneous activity and large-amplitude optogenetic hyperpolarization (green bar) leading to rebound excitation (arrows). (**c**) Synaptic responses of a SPN to a pause-excitation population response of ChAT interneurons. Top, rebound excitation of the interneurons triggered coincident large IPSPs (arrow) that efficiently blocked action potential generation. Middle, spike trains of ChAT interneurons recorded using cell-attached (asterisks) and extracellular (arrowheads) recording (second trace from top) and in current clamp (color traces). Inset, eNpHR3.0-YFP–expressing ChAT interneurons

and cell-attached recording pipettes (red). Bottom, PSTH of ChAT interneurons demonstrating pronounced pause-excitation activity. (**d**) Simultaneous current recordings (blue and red) from two SPNs showing IPSCs elicited by the rebound activation of ChAT interneurons (bottom) induced using eNpHR1.0-mCherry. Simultaneous voltage recording from a third SPN showed optically elicited spike delay (top, arrow). Bottom, extracellular recording of a ChAT interneuron (spikes, vertical lines) showed optical inhibition and rebound firing. (**e**) Top, short and long latency inhibition (black trace, red and blue arrows) in a SPN elicited by ChAT interneurons were blocked by DHβE (red traces). Bottom, cell-attached recording demonstrated long latency spikes in a ChAT interneuron (arrows) coinciding with late inhibition. Note that the early inhibition is elicited by other ChAT interneurons.
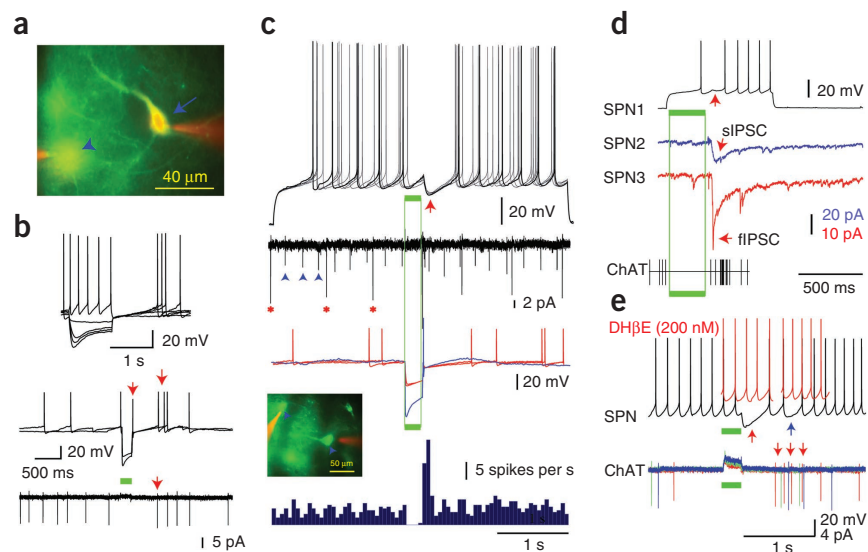
Figure 6 Pause-excitation sequences of ChAT interneurons inhibit SPNs *in vivo* in freely moving mice. (**a**) Left, waveforms of distinct types of units included in analysis. Average unit waveform is shown in gray, population averages are in color. Overlay demonstrates feature differences between unit types. Right, firing rates (mean ± s.e.m.) of the three types of units. SPNs exhibited significantly lower firing rates than other unit types (*t* test, *P* < 0.01). (**b**) Examples of spike trains of putative SPNs and ChAT interneurons. Note that a bursting episode was selected for the SPN. (**c**) Characteristics of the population response of ChAT interneurons elicited with optogenetic inhibition. Note the instantaneous inhibition of firing and the excitation phase that is similar to the responses of putative ChAT interneurons in primates (bins, 30 ms). (**d**) Inhibition of firing of SPNs (bottom three PSTHs) by pause-excitation activity pattern of ChAT interneurons (top). Lower three PSTHs show (respectively, from top to bottom) cumulative response of all SPNs, SPN responses following 200-ms optical inhibition and responses following 1,000-ms inhibition. The population mean and 2 s.d. below the mean firing rates are indicated by blue and red lines, respectively. Note that the end of the optical stimulus was closely followed by strong inhibition of firing in SPNs. Consecutive bins with firing rates more than 2 s.d. below the mean are indicated by bins colored in blue. Note that the optical inhibition itself did not elicit an observable firing rate change in the SPNs. Horizontal bars denote periods of illumination (bins, 50 ms).
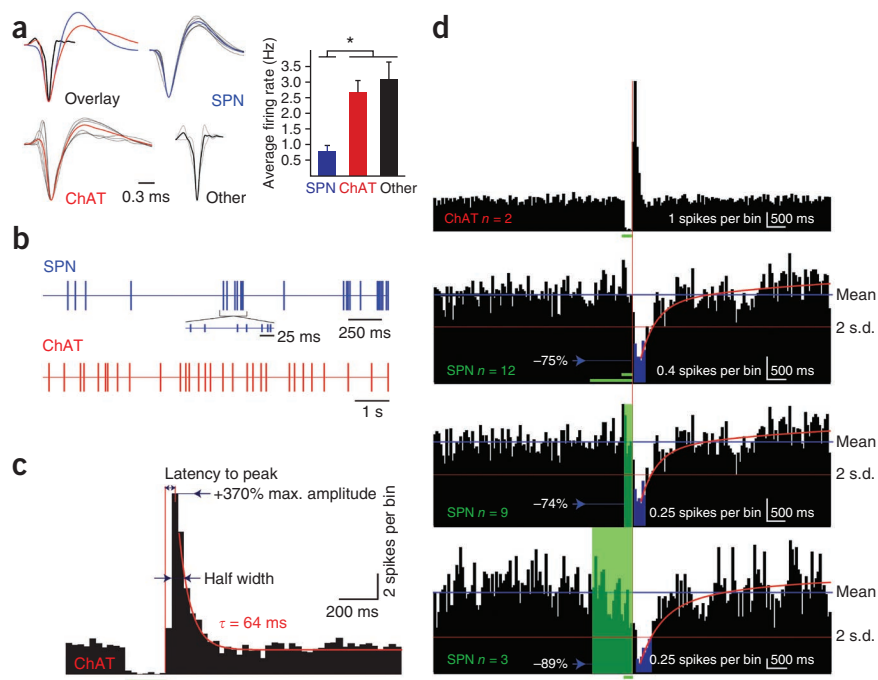
stimulus was a 200-ms (*n* = 9) or a 1,000-ms (*n* = 3) laser pulse (10–30 mW, 594 nm) delivered at fixed 20-s or 30-s intervals. None of the mice exhibited observable behavioral responses to the delivery of light pulses. Units were separated and classified as described in the Online Methods (**Fig. 6a**). The identity of ChAT interneurons was directly confirmed on the basis of zero time-lag optical inhibition.

Six isolated ChAT units were identified in four animals. These neurons exhibited irregular tonic activity that was similar to the firing pattern of putative ChAT interneurons that has been described in primates and to optogenetically identified ChAT interneurons in the nucleus accumbens[32] (**Fig. 6b**). A 200-ms optical inhibition elicited a pause-excitation sequence that was characterized by nearly complete silencing during illumination followed by rebound firing (**Fig. 6c**). The rebound population activity lasted approximately 150 ms and exhibited a maximal firing rate of 370% of baseline that occurred about 45 ms after the offset of the stimulus and recovered exponentially with a time constant of 64 ms (**Fig. 6c**). The overall response and the characteristics of rebound excitation closely recapitulated the key properties of putative ChAT interneuron population responses recorded in a variety of behavioral procedures[3,4,8,30].

The same optical stimuli elicited powerful inhibition of firing in putative SPNs, including 7 isolated and 5 multiunit recordings of these neurons (**Fig. 6d**). The inhibition exhibited a rapid onset (112.5 ± 90.8–ms delay from the end of the light to pulse to the first 50-ms peristimulus time histogram (PSTH) bin more than 2 s.d. below the mean). The mean maximal inhibition was 84.7 ± 15.3% (defined as the mean firing rate reduction during the two most strongly inhibited consecutive bins), representing a significant change (*P* = 0.0019, see Online Methods) for each putative SPN. Note that the smaller magnitude of the maximal inhibition of the SPN population activity (74%; **Fig. 6d**) was a result of averaging of multiple responses with different response latencies. The firing rate remained more than 2 s.d. below the mean for 200 ± 85.3 ms and recovered bi-exponentially

from its minimal value with time constants of 190 ms (64% of peak) and 0.4 s (36% of peak, *n* = 12). To confirm that the coincidence of the onset of the inhibition and the end of the light pulse reflected a causal relationship, we also tested the effect of 1,000-ms (*n* = 3) light pulses. The inhibitory responses elicited by these stimuli were similarly timed to the end of the stimuli (**Fig. 6d**). Notably, there was no observable firing rate change in the same units during either 200- or 1,000-ms optical inhibition of ChAT interneurons (**Fig. 6d**). Finally, inhibition resembling the responses of putative SPNs was also observed in two units that exhibited firing rates and waveforms different from putative SPNs (**Fig. 6a**), suggesting that some GABAergic interneurons may be regulated similarly to SPNs (**Supplementary Fig. 9**).

DISCUSSION

Our findings suggest the existence of multiple GABAergic circuits that are activated by ChAT interneurons and examine their role in the regulation of the activity of SPNs. The detailed organization of these circuits remains incompletely understood. We found that NPY-NGF interneurons were directly activated by nicotinic synaptic input and elicited slow GABAeric inhibition in SPNs. The electrophysiological and circuitry properties of NPY-NGF interneurons appeared to be well suited for transmitting cholinergic population responses. Specifically, the slow time course of the nEPSP is expected to facilitate integration of synaptic inputs during semi-synchronous activation of ChAT interneurons, whereas the high current threshold and the feedforward inhibition of NPY-NGF interneurons may prevent their spurious activation by randomly coincident presynaptic inputs. Furthermore, the utilization of $GABA_A$ slow, which, on the basis of experiments using low-affinity antagonists[15], subtype-specific modulators[12,14,15,33], diffusional interference[15] and blockade of GABA transport[14–16], appears to involve volume transmission and the activation of extrasynaptic receptors[33,34], enabled high-fidelity, widespread inhibition of large neuron populations by single presynaptic elements.

These characteristics, together with the extremely high probability of connectivity and electrotonic coupling of NPY-NGF neurons support uniform inhibition of SPNs, despite the relatively small population size of these interneurons[18].

Our biophysical and pharmacological evidence also support the cholinergic activation of a second, separate GABAergic input to SPNs that is responsible for the fIPSC. The possibility that the fIPSC is generated by direct synaptic contacts of NPY-NGF neurons onto SPNs, whereas the sIPSC originates through volume transmission of GABA released from a larger set of terminals of the same interneurons, is inconsistent with the observation that, in a large number of paired recordings of NPY-NGF interneurons and SPNs ($n = 40$, 11 from this study and 29 from our earlier report[18]), no fIPSC components have been observed. Presynaptic nicotinic facilitation or GABA release could mediate the fIPSC[35–37], possibly involving terminals of FSIs that express nicotinic receptors, but a presynaptic mechanism is inconsistent with the absence of an asynchronous barrage of mini-IPSCs during the compound response[35,36]. However, presynaptic facilitation of GABA release from synapses responsible for the sIPSC cannot be excluded, and this mechanism could account for the IPSCs elicited in SPNs by single ChAT interneurons. Thus, the simplest hypothesis regarding the origin of the fIPSC is that it is elicited by action potential firing in a type of GABAergic interneuron that is distinct from NPY-NGF, NPY-PLTS and fast-spiking neurons. The most likely candidates are calretinin-expressing[38] and tyrosine hydroxylase–expressing interneurons[39]. Similarly, the recurrent inhibition of ChAT interneurons is also likely to originate from a subset of calretinin- or tyrosine hydroxylase–expressing interneurons that appear to be distinct from those mediating the fIPSC. ChAT interneurons form a complex network with their GABAergic postsynaptic partners that includes two different inhibitory feedback mechanisms, electrical coupling between NPY-NGF neurons and inhibition among some of the GABAergic interneurons themselves. This network may be important for shaping and processing the transient population responses of ChAT interneurons and may contribute to the generation and behaviorally contingent frequency transitions of gamma-range oscillations in the neostriatum[40].

We also investigated the effect of a physiologically realistic pause-excitation activity pattern of ChAT interneurons on the spontaneous firing of putative SPNs in freely moving mice. SPNs exhibited a rapidly developing, powerful inhibitory response that coincided with the synchronous firing of ChAT interneurons, confirming our *in vitro* results. Notably, brief (<1 s) silencing of ChAT interneurons did not elicit an observable effect, suggesting the absence of tonic muscarinic modulation of SPNs, their synaptic inputs[23,26] or sustained nicotinic receptor–driven GABAergic inhibition. Thus, the pause response of ChAT interneurons may not affect striatal function primarily through the regulation of the firing of SPNs, but may instead involve other mechanisms, including reversal of the permissive nicotinic facilitation of dopamine release[41,42]. A potential involvement of more complex muscarinic effects[26] cannot be ruled out on the basis of our results. In addition, the *in vivo* and *in vitro* responses of SPNs to manipulation of ChAT interneuron activity were different in the dorsal striatum from those described previously in the nucleus accumbens[32], suggesting that there are substantial differences in the circuit organization of these two brain areas.

From a behavioral perspective, feedforward inhibition of SPNs by ChAT interneurons may contribute to the interruption and reorientation of ongoing behavior when salient stimuli are encountered. Synchronous activation of ChAT interneurons by intralaminar thalamic inputs that carry information about alerting stimuli[43] is expected to trigger feedforward inhibition of SPNs and interrupt the ongoing activity of cortico-basal ganglia loops. Furthermore, feedforward inhibition may aid adaptive reorientation of behavior by promoting preferential reactivation of specific SPNs and cortico-basal ganglia circuits that are responsive to the thalamo-striatal excitatory inputs that are activated by the alerting stimuli. The targeting of SPNs by the same excitatory thalamic input responsible for synchronous cholinergic activation may also explain why inhibition of the firing of SPNs is less consistently observed during naturally occurring than during optogenetically elicited synchronous activity of ChAT interneurons in behaving animals[44]. Notably, as ChAT interneurons respond primarily to stimuli with conditioned reinforcement value, the feedforward inhibitory circuit can selectively gate the effect of external stimuli on ongoing behavior depending on the behavioral importance of these stimuli. Finally, the inhibitory circuits described here may causally link the partial loss of ChAT interneurons[45] and the motor symptoms of Tourette syndrome, as has previously been hypothesized[46].

METHODS

Methods and any associated references are available in the online version of the paper at http://www.nature.com/natureneuroscience/.

Note: Supplementary information is available on the Nature Neuroscience website.

AUTHOR CONTRIBUTIONS
D.F.E. carried out all of the *in vivo* recording experiments and data analysis, performed the majority of the *in vitro* experiments, and contributed to virus production, virus injections and confocal imaging (with the exception of **Fig. 1a**, which was produced by J. Berlin). O.I.-S. and F.T. performed the initial *in vitro* analysis of NPY-NGF neurons and O.I.-S. identified nicotinic synapses in these interneurons. E.S. contributed to the design of *in vivo* recording, optical stimulation methods and data analysis, molecular biology, and virus production. G.B. contributed to optrode design and the design and analysis of *in vivo* recording experiments. K.D. designed and provided constructs for optogenetic expression vectors, designed and produced the *AAV5-DIO-eNpHR3.0-YFP* and the *AAV5-DIO-ChR2-mCherry* virus vectors, and contributed to optogenetic methods. J.M.T. contributed to the development of *in vitro* and *in vivo* recording methods. T.K. performed *in vitro* recordings, recombinant DNA procedures and lentivirus production. The study was designed by T.K., J.M.T. and D.F.E. and the manuscript was written by T.K. with substantial contributions from D.F.E. and J.M.T. and input from all of the authors.

COMPETING FINANCIAL INTERESTS
The authors declare no competing financial interests.

Published online at http://www.nature.com/natureneuroscience/.
Reprints and permissions information is available online at http://www.nature.com/reprints/index.html.

1. Graybiel, A.M. The basal ganglia and chunking of action repertoires. *Neurobiol. Learn. Mem.* **70**, 119–136 (1998).
2. Schultz, W. Predictive reward signal of dopamine neurons. *J. Neurophysiol.* **80**, 1–27 (1998).
3. Morris, G., Arkadir, D., Nevet, A., Vaadia, E. & Bergman, H. Coincident but distinct messages of midbrain dopamine and striatal tonically active neurons. *Neuron* **43**, 133–143 (2004).
4. Joshua, M., Adler, A., Mitelman, R., Vaadia, E. & Bergman, H. Midbrain dopaminergic neurons and striatal cholinergic interneurons encode the difference between reward and aversive events at different epochs of probabilistic classical conditioning trials. *J. Neurosci.* **28**, 11673–11684 (2008).

5. Hyland, B.I., Reynolds, J.N., Hay, J., Perk, C.G. & Miller, R. Firing modes of midbrain dopamine cells in the freely moving rat. *Neuroscience* **114**, 475–492 (2002).
6. Kimura, M., Rajkowski, J. & Evarts, E. Tonically discharging putamen neurons exhibit set-dependent responses. *Proc. Natl. Acad. Sci. USA* **81**, 4998–5001 (1984).
7. Apicella, P. Leading tonically active neurons of the striatum from reward detection to context recognition. *Trends Neurosci.* **30**, 299–306 (2007).
8. Aosaki, T. *et al.* Responses of tonically active neurons in the primate's striatum undergo systematic changes during behavioral sensorimotor conditioning. *J. Neurosci.* **14**, 3969–3984 (1994).
9. Aosaki, T., Kimura, M. & Graybiel, A.M. Temporal and spatial characteristics of tonically active neurons of the primate's striatum. *J. Neurophysiol.* **73**, 1234–1252 (1995).
10. Tecuapetla, F., Koos, T., Tepper, J.M., Kabbani, N. & Yeckel, M.F. Differential dopaminergic modulation of neostriatal synaptic connections of striatopallidal axon collaterals. *J. Neurosci.* **29**, 8977–8990 (2009).
11. Pearce, R.A. Physiological evidence for two distinct GABAA responses in rat hippocampus. *Neuron* **10**, 189–200 (1993).
12. Banks, M.I., Li, T.B. & Pearce, R.A. The synaptic basis of $GABA_{A,slow}$. *J. Neurosci.* **18**, 1305–1317 (1998).
13. Tamás, G., Lorincz, A., Simon, A. & Szabadics, J. Identified sources and targets of slow inhibition in the neocortex. *Science* **299**, 1902–1905 (2003).
14. Karayannis, T. *et al.* Slow GABA transient and receptor desensitization shape synaptic responses evoked by hippocampal neurogliaform cells. *J. Neurosci.* **30**, 9898–9909 (2010).
15. Szabadics, J., Tamas, G. & Soltesz, I. Different transmitter transients underlie presynaptic cell type specificity of $GABA_{A,slow}$ and $GABA_{A,fast}$. *Proc. Natl. Acad. Sci. USA* **104**, 14831–14836 (2007).
16. Banks, M.I., White, J.A. & Pearce, R.A. Interactions between distinct $GABA_A$ circuits in hippocampus. *Neuron* **25**, 449–457 (2000).
17. Overstreet, L.S., Jones, M.V. & Westbrook, G.L. Slow desensitization regulates the availability of synaptic $GABA_A$ receptors. *J. Neurosci.* **20**, 7914–7921 (2000).
18. Ibáñez-Sandoval, O. *et al.* A novel functionally distinct subtype of striatal neuropeptide Y interneuron. *J. Neurosci.* **31**, 16757–16769 (2011).
19. Gittis, A.H., Nelson, A.B., Thwin, M.T., Palop, J.J. & Kreitzer, A.C. Distinct roles of GABAergic interneurons in the regulation of striatal output pathways. *J. Neurosci.* **30**, 2223–2234 (2010).
20. Capogna, M. & Pearce, R.A. $GABA_{A,slow}$: causes and consequences. *Trends Neurosci.* **34**, 101–112 (2011).
21. Hill, J.A. Jr., Zoli, M., Bourgeois, J.P. & Changeux, J.P. Immunocytochemical localization of a neuronal nicotinic receptor: the beta 2-subunit. *J. Neurosci.* **13**, 1551–1568 (1993).
22. Koós, T. & Tepper, J.M. Inhibitory control of neostriatal projection neurons by GABAergic interneurons. *Nat. Neurosci.* **2**, 467–472 (1999).
23. Koós, T. & Tepper, J.M. Dual cholinergic control of fast-spiking interneurons in the neostriatum. *J. Neurosci.* **22**, 529–535 (2002).
24. Chang, H.T. & Kita, H. Interneurons in the rat striatum: relationships between parvalbumin neurons and cholinergic neurons. *Brain Res.* **574**, 307–311 (1992).
25. Sullivan, M.A., Chen, H. & Morikawa, H. Recurrent inhibitory network among striatal cholinergic interneurons. *J. Neurosci.* **28**, 8682–8690 (2008).
26. Ding, J.B., Guzman, J.N., Peterson, J.D., Goldberg, J.A. & Surmeier, D.J. Thalamic gating of corticostriatal signaling by cholinergic interneurons. *Neuron* **67**, 294–307 (2010).
27. Giniatullin, R., Nistri, A. & Yakel, J.L. Desensitization of nicotinic ACh receptors: shaping cholinergic signaling. *Trends Neurosci.* **28**, 371–378 (2005).
28. Wilson, C.J. The mechanism of intrinsic amplification of hyperpolarizations and spontaneous bursting in striatal cholinergic interneurons. *Neuron* **45**, 575–585 (2005).
29. Gradinaru, V. *et al.* Molecular and cellular approaches for diversifying and extending optogenetics. *Cell* **141**, 154–165 (2010).
30. Apicella, P., Ravel, S., Sardo, P. & Legallet, E. Influence of predictive information on responses of tonically active neurons in the monkey striatum. *J. Neurophysiol.* **80**, 3341–3344 (1998).
31. Gradinaru, V., Thompson, K.R. & Deisseroth, K. eNpHR: a *Natronomonas* halorhodopsin enhanced for optogenetic applications. *Brain Cell Biol.* **36**, 129–139 (2008).
32. Witten, I.B. *et al.* Cholinergic interneurons control local circuit activity and cocaine conditioning. *Science* **330**, 1677–1681 (2010).
33. Oláh, S. *et al.* Regulation of cortical microcircuits by unitary GABA-mediated volume transmission. *Nature* **461**, 1278–1281 (2009).
34. Banks, M.I. & Pearce, R.A. Kinetic differences between synaptic and extrasynaptic GABA(A) receptors in CA1 pyramidal cells. *J. Neurosci.* **20**, 937–948 (2000).
35. Wonnacott, S. Presynaptic nicotinic ACh receptors. *Trends Neurosci.* **20**, 92–98 (1997).
36. McGehee, D.S., Heath, M.J., Gelber, S., Devay, P. & Role, L.W. Nicotine enhancement of fast excitatory synaptic transmission in CNS by presynaptic receptors. *Science* **269**, 1692–1696 (1995).
37. De Rover, M., Lodder, J.C., Schoffelmeer, A.N. & Brussaard, A.B. Intermittent morphine treatment induces a long-lasting increase in cholinergic modulation of GABAergic synapses in nucleus accumbens of adult rats. *Synapse* **55**, 17–25 (2005).
38. Kubota, Y., Mikawa, S. & Kawaguchi, Y. Neostriatal GABAergic interneurones contain NOS, calretinin or parvalbumin. *Neuroreport* **5**, 205–208 (1993).
39. Ibáñez-Sandoval, O. *et al.* Electrophysiological and morphological characteristics and synaptic connectivity of tyrosine hydroxylase–expressing neurons in adult mouse striatum. *J. Neurosci.* **30**, 6999–7016 (2010).
40. Berke, J.D. Fast oscillations in cortical-striatal networks switch frequency following rewarding events and stimulant drugs. *Eur. J. Neurosci.* **30**, 848–859 (2009).
41. Zhou, F.M., Liang, Y. & Dani, J.A. Endogenous nicotinic cholinergic activity regulates dopamine release in the striatum. *Nat. Neurosci.* **4**, 1224–1229 (2001).
42. Rice, M.E. & Cragg, S.J. Nicotine amplifies reward-related dopamine signals in striatum. *Nat. Neurosci.* **7**, 583–584 (2004).
43. Matsumoto, N., Minamimoto, T., Graybiel, A.M. & Kimura, M. Neurons in the thalamic CM-Pf complex supply striatal neurons with information about behaviorally significant sensory events. *J. Neurophysiol.* **85**, 960–976 (2001).
44. Hikosaka, O., Sakamoto, M. & Usui, S. Functional properties of monkey caudate neurons. III. Activities related to expectation of target and reward. *J. Neurophysiol.* **61**, 814–832 (1989).
45. Kataoka, Y. *et al.* Decreased number of parvalbumin and cholinergic interneurons in the striatum of individuals with Tourette syndrome. *J. Comp. Neurol.* **518**, 277–291 (2010).
46. Leckman, J.F., Vaccarino, F.M., Kalanithi, P.S. & Rothenberger, A. Annotation: Tourette syndrome: a relentless drumbeat driven by misguided brain oscillations. *J. Child Psychol. Psychiatry* **47**, 537–550 (2006).

ONLINE METHODS

Transgenic mice. Cholinergic interneurons were targeted in homozygotic *Chat-IRES-cre* transgenic mice (*B6;129S6-Chat<tme1(cre)Lowl>/J*, Jackson Laboratory). The role of NPY interneurons was examined in double transgenic mice generated by cross breeding the *Chat-IRES-cre* strain with a *B6.FVB-Tg(NPY-hrGFP)1Lowl/J* strain (Jackson Laboratory). GFP targeted paired recording from ChAT interneurons and SPNs was performed using *B6.Cg-Tg(RP23-268L19-EGFP)2Mik/J* mice (Jackson Laboratory). All experiments were conducted with the approval of the Rutgers University Institutional Animal Care and Use Committee.

Production of AAV-2, AAV-5 and integration deficient lentivirus vectors. Adeno-associated virus serotype 2 (AAV-2) was used for the expression of ChR2-YFP and serotype 5 (AAV-5) virus for eNpHR3.0-YFP and ChR2-mCherry. The AAV-2 vector was produced at Vector Biolabs using transfer vector DNA generated by K.D. The AAV-5 vectors were produced by the vector core of the University of North Carolina. The transfer vector plasmids and the transgene constructs were designed by K.D. (http://www.stanford.edu/group/dlab/optogenetics/sequence_info.html).

Lentivirus mediated, Cre/*loxP* controlled expression of eNpHR1.0-mCherry was carried out with integration deficient lentiviral (IDL) particles to prevent chromosomal rearrangements that may occur across multiple proviral *loxP* or *lox2227* recombination sites when integrating virus is employed. IDL particles were produced in 293FT cells (Invitrogen) grown to 95–100% confluence in DMEM (+10% fetal bovine serum (vol/vol) and 1% L-glutamine (vol/vol)) using TransIT-293 (Mirus) transfection agent as described previously[47]. Briefly, confluent 293FT cells in each of six 175-cm^2 flasks (Falcon) were co-transfected with 22 µg of the lentiviral transfer vector DNA (*pLenti:EF1:DOI:eNpHR1.0-mCherry:WPRE*) and the second generation packaging plasmids *pCMV-dR8.74-D64V* (15 µg), and *pMD2.G* 5 µg; (Addgene, 12259) supplemented with a plasmid carrying a suppressor of a dsRNA inhibitor (*pAdvantage*, Promega, 2 µg). The *pCMV-dR8.74-D64V* plasmid encodes the lentiviral integrase carrying a D64V point mutation that completely blocks proviral integration[48] and was a gift from R. Yanez-Munoz (Royal Holloway-University of London). The medium was changed to a viral production medium (Ultraculture, Lonza, + 1% pen-strep (vol/vol), 1% sodium pyruvate (vol/vol), and 5 mM sodium butyrate) 24 h after transfection, and the virus-containing supernatant was collected and concentrated with ultracentrifugation 48 h post-transfection. The titer of the concentrated IDL particles was not directly determined, but comparison with lentivirus stocks of known titer injected in mouse brains indicated that it approached 10^9 IU ml^{-1}.

The *eNpHR1.0-mCherry* transgene was produced by adding the endoplamisc reticulum export and plasma membrane localization signals described previously[31] in two rounds of extension PCR using a high-fidelity DNA polymerase (Accupime *Pfx*, Invitrogen) to the coding sequence of *NpHR-mCherry* produced by K.D. (http://www.stanford.edu/group/dlab/optogenetics/sequence_info.html). The primer sequences for the first and second PCR rounds were, respectively, 5′-GTCGTCTCTCTGTTCTCTCTGCTTCAGGACACAGAGACCCTGCCTCCCGTGACCGAGAGT-3′ and 5′-TTACACCTCGTTCTCGTAGCAGAACTTGTACAGCTCGTCCATGC-3′, and 5′-GGCCTGCGCTAGCGCCACCATGAGGGGTACGCCCCTGCTCCTCGTCGTCTCTCTGTTCTCTCTGCTTCAG-3′ and 5-′CGGACCCATATGGGCGCGCCTTACACCTCGTTCTCGT-3′. The PCR product was subcloned in an inverted orientation between the *loxP/lox2722* flanking recombination sites, replacing the ChR2-YFP coding sequence in an *AAV:EF1:DOI:ChR2-YFP:WPRE* plasmid from which the entire expression cassette (*EF1:DOI:eNpHR1.0-mCherry:WPRE*) was subsequently cloned into a third generation (Tat independent) self-inactivating lentiviral expression vector. Detailed map is available on request.

Intracerebral virus injection. All *in vivo* and *in vitro* surgical procedures were performed in accordance with the US National Institutes of Health *Guide to the Care and Use of Laboratory Animals* and with the approval of the Rutgers University Institutional Animal Care and Use Committee. The virus injection surgeries were performed in a custom-built surgical setup inside an isolation cabinet under Biosafety Level-2 (BL-2) confinement. Mice were anesthetized with isoflurane and the skull was exposed under antiseptic conditions using local anesthesia with bupivacaine. A small burr hole was drilled at coordinates 0.5–1.0 mm anterior to Bregma, 1.5–2.2 mm lateral. We injected 0.5–1.5 µl of concentrated virus stock solution using a Nanoject-2 pressure injection apparatus and glass pipettes over 10–40 min at a depth of 2.4–2.7 mm from the surface of the brain. Animals were housed in a BL-2 safety cabinet for at least 6 d. Experiments were conducted 7–30 d following injection.

Immunocytochemistry. Fixation was performed after establishing anesthesia with ketamine (400 mg per kg of body weight, intraperitoneal) with transcardial perfusion using 10 ml of ice-cold oxygenated Ringer solution followed by 75–100 ml of 4% paraformaldehyde (wt/vol) and 15% saturated picric acid (vol/vol) in 0.15 M phosphate buffer. Brains were kept in the same fixative overnight. We cut 60-µm sections on a Vibratome. The immunocytochemical labeling of ChAT included pre-incubation in 10% methanol (vol/vol) and 3% hydrogen peroxide (vol/vol) in phosphate-buffered saline (PBS), blocking of nonspecific binding with 10% normal donkey serum (vol/vol), 3% bovine serum albumin (vol/vol) in a 0.5% Triton X-100 solution (vol/vol) in PBS, followed by incubation in the blocking solution containing goat antibody to ChAT (1:200, cat. #AB144P, Millipore) for 48 h at 20–25 °C. After wash, sections were incubated in donkey antibody to goat IgG conjugated to Alexa-594 (1:100) in PBS at 20–25 °C overnight. Sections were mounted in Vectashield medium.

***In vitro* optical stimulation.** ChR2-YFP was activated using a 750-mW blue LED (http://www.cree.com/) with light projected onto the slice through the condenser of the microscope with the bottom differential interference contrast polarizer removed. The intensity and duration of the illumination were controlled through a digital to analogue converter output of a ITC-18 digitizer and a Mightex SLA LED driver. eNpHR3.0-YFP and eNpHR1.0-mCehrry were activated with alternating pulses of 200–300-ms green (514 ± 20 nm) and blue (470 ± 20 nm) light delivered through the epifluorescence illumination pathway using Chroma Technologies filter cubes under temporal control with a Uniblitz shutter (Vincent Associates). Blue light was delivered to facilitate recovery from photodesensitization. Optical stimuli were delivered at 30–60-s intervals to allow recovery to baseline.

***In vivo* optical stimulation.** We chronically implanted 125-µm multi-mode optic fibers (part #AFS105/125Y, Thor Labs) as part of the optrode. To minimize tissue damage and increase the lateral distribution of light, we etched optical fibers by immersing ~200 µm of the tip of the fiber in hydrofluoric acid (Sigma-Aldrich) overlaid with mineral oil and then slowly lifting the fiber tip into the protective oil layer (over ~30–60 min), resulting in a smooth, gradual taper and a tip diameter of <50 µm. Implanted fibers were coupled to a 594-nm DPSS laser (LaserGlow Technologies) via modified light-coupling connectors (part # 86024-5500, Thor Labs) and ceramic attachments encasing the external end of the fiber. Light intensity at the fiber tip was measured before implantation as 10–30 mW. Illumination duration was controlled via a TTL-gated shutter with a transition time of less than 0.5 ms (Uniblitz LS2; Vincent Associates). Stimulation timing was controlled via Spike2 software running a CED micro MKII Digitizer (software and hardware were from Cambridge Electronic Design).

***In vitro* slice preparation and recording.** Transgenic mice were 60–390 d old when killed. Brain slices were prepared and visualized whole-cell recordings were performed as described previously[10]. Voltage-clamp recordings were performed with a CsCl-based medium in some cases including QX-314 (5–15 mM). Action potentials were elicited in ChAT interneurons usually in voltage clamp with 3–5-ms, 70–100-mV pulses. These recordings used KCl-based internal solution with E[Cl$^-$] ≈ −10 mV to facilitate detection of recurrent IPSCs. Most neurons were intracellularly labeled with Alexa-594 or Alexa-488 (25–75 µM).

Chronic *in vivo* extracellular recording. Optrodes were composed of four independently movable tetrodes mounted in a five cannula array surrounding a central optic fiber with lateral distances between the five elements set at 200 µm. Tetrode wires were gold-plated to impedances of <400 kOhm measured at 1 kHz, no more than 1 h before implantation. Coordinates targeting dorsal striatum were +0.5–1.0 mm anterior, 1.6–2.0 mm lateral and −2.4–2.7 mm ventral (relative to Bregma). Animals were implanted with optrodes >7 d post virus injection.

Wires were advanced slowly until units were encountered. The recorded extracellular potential was pre-amplified 20× using a headstage pre-amplifier (Plexon) and further amplified 100× and band-pass filtered (0.1–10,000 Hz) using an analog amplifier (Grass Technologies), digitized at 25 kHz (micro MKII Digitizer,

Cambridge Electronic Design) and recorded for off-line analysis using Spike2 software (Cambridge Electronic Design).

Analysis of *in vitro* data. Analysis was performed in Axograph2.0 (J. Clements) or with routines written in IgorPro (WaveMetrics). Rise times were defined as the time difference between the data points at which the amplitude of the response was 10% and 90% of peak. For the analysis of the correlation of fIPSC and sIPSC amplitudes, individual response amplitudes were defined as the mean in a 1-ms (fIPSC) or 15–35-ms (sIPSC) window (**Fig. 1f**). The wide window averaging was carried out to eliminate the contribution of the uncorrelated stochastic channel noise associated with the sIPSC. An exponential function was then fitted to the fIPSC and sIPSC amplitudes of subsequent compound responses expressed as functions of recording time, which revealed that both amplitudes decayed over repeated stimulations. The exponentially fitted trend of amplitude decay was then subtracted from the individual amplitudes and the de-trended amplitudes were expressed relative to the respective average fIPSCs and sIPSCs amplitudes, thus defining ΔfIPSC and ΔsIPSC (**Fig. 1f**). This procedure removes a source of correlated variance of unknown origin, but the uncorrelated nature of the residual variance excludes in itself the possibility of shared receptor mechanisms or neurotransmitter pools underlying the two response components.

Analysis of *in vivo* data. Spike2 software was used for spike detection and sorting. Signals were band-pass filtered (300–6,000 Hz, digital two-pole Butterworth filter) and an appropriate spike trigger threshold was set by the experimenter (approximately 3–5 times the s.d. of the noise). Wavemarks defined as 0.5-ms pre and 1.0-ms post peak threshold crossing were extracted from each channel when at least one channel was triggered. After detection, the mean of the peak amplitudes (negative going) on the four channels was measured and this data was combined with the relative ratios of the peaks on the four channels, yielding five variables, from which three principal components were extracted using a principal component analysis routine of Spike2. The events were then projected in a thus defined three-dimensional space and were automatically over-clustered using the K-mean statistics (10–20 clusters are initially cut for data actually having less than five units). Clusters that were manually classified as noise on the basis of waveform shapes and inter-stimulus interval (ISI) histograms were discarded. The remaining potential units were then recombined and reclassified the same way a second time, with the effect of reducing the bias introduced in the first iteration by the noise and improving the extraction of principal components most discriminative among extracellular spikes. The identified clusters were then subjected to principal component analysis based on multidimensional data defined by all amplitude values in the spike waveforms. K-means were again used to automatically

over-cluster the data, and the clustering information from waveforms and relative amplitude ratios was reconciled manually. Auto and cross-correlation histograms were constructed and units were classified as putative single units if there was a clear refractory period (>3 ms) and if, in the ISI histogram, 10% or less of the spikes in the first 50 ms occurred in the first 5 ms (ref. 49). Unit clusters that had classifiable waveforms similar to single units, but did not meet these criteria were classified as multiple unit recordings.

Differences in waveform shape and firing pattern as well as optical responses were used to classify cell types. In accordance with previous reports, putative SPN single units had firing rates <2 Hz (mean = 0.74 Hz, s.d. = 0.62) and band-pass filtered (300–6,000 Hz) waveform valley widths >0.35 ms (mean = 0.51 ms, s.d. = 0.09)[50]. ChAT units were identified based on zero latency optical inhibition. Notably, the waveforms of ChAT and SPN units were similar, the most reliable difference being an initial positive phase present in most ChAT units (**Fig. 6**). Spikes of ChAT units fired tonically whereas SPNs tended to fire single spikes or bursts interspersed with long (>1 s) periods of silence. Units classified as 'other neurons' had firing rates similar to ChAT interneurons, but had significantly shorter waveforms than all other unit classes and their firing rate was not directly modulated by illumination.

To examine the relationship between optical stimulation and changes in the firing rate of SPNs, PSTHs were constructed using 50-ms binning and the mean and the s.d. of the spike number per bin were calculated for the 10–20 s preceding the stimulus (20–40 bins). A statistically significant change in firing rate change was defined as two consecutive bins outside mean ± 2 s.d., defining a significance level of $P = 0.0019$.

Statistical methods. Given the small number of observations in most cases, the nonparametric Wilcoxon rank-sum test was used to compare the means of populations. These calculations and linear regression analysis were performed in IgorPro or StatView. Population measurements are reported as mean ± s.d. unless otherwise indicated. The statistical significance of firing rate changes *in vivo* were determined as described above.

47. Han, X. *et al.* Millisecond-timescale optical control of neural dynamics in the nonhuman primate brain. *Neuron* **62**, 191–198 (2009).
48. Yáñez-Muñoz, R.J. *et al.* Effective gene therapy with nonintegrating lentiviral vectors. *Nat. Med.* **12**, 348–353 (2006).
49. Jog, M.S. *et al.* Tetrode technology: advances in implantable hardware, neuroimaging, and data analysis techniques. *J. Neurosci. Methods* **117**, 141–152 (2002).
50. Berke, J.D. Uncoordinated firing rate changes of striatal fast-spiking interneurons during behavioral task performance. *J. Neurosci.* **28**, 10075–10080 (2008).